

N ν DEx-100 Conceptual Design Report

N ν DEx-100 collaboration

X. Cao,^a Y. Chang,^b K. Chen,^c E. Ciuffoli,^d L. Duan,^d D. Fang,^d C. Gao,^c S. K. Ghorui,^d P. Hu,^b Q. Hu,^d Z. Huang,^b L. Lang,^c Y. Li,^e Z. Li,^d T. Liang,^c J. Liu,^c C. Lu,^d F. Mai,^d Y. Mei,^f H. Qiu,^{d,1} X. Sun,^c X. Tang,^e H. Wang,^c Q. Wang,^b L. Xiao,^c M. Xiao,^d J. Xin,^b N. Xu,^{d,f} P. Yang,^d Y. Yang,^d Z. Yang,^d Z. Yu,^c D. Zhang,^c J. Zhang,^g C. Zhao,^d D. Zhu^c

^a*Shanghai Advanced Research Institute, Chinese Academy of Sciences, Shanghai 201210, China*

^b*Lanzhou University, 222 South Tianshui Road, Lanzhou, China*

^c*Central China Normal University, 152 Luoyu Road, Wuhan, China*

^d*Institute of Modern Physics, Chinese Academy of Sciences, 509 Nanchang Rd., Lanzhou, China*

^e*Shanghai Institute of Applied Physics, Chinese Academy of Sciences, Shanghai 201800, China*

^f*Lawrence Berkeley National Laboratory, 1 Cyclotron Rd, Berkeley, CA, USA*

^g*North China University of Water Resources and Electric Power, 36 Beihuan Road, Zhengzhou, China*

E-mail: qiuuh@impcas.ac.cn

ABSTRACT: The measurement of nuclear neutrinoless double-beta ($0\nu\beta\beta$) decay would be a revolutionary result in particle physics. The observation of such a decay would prove that the neutrinos are their own antiparticles, help to study the absolute mass of neutrinos, explore the origin of their mass, and may explain the matter-antimatter asymmetry in our universe by the violation of lepton number.

We propose to develop a time projection chamber (TPC) using high-pressure $^{82}\text{SeF}_6$ gas and the top-metal silicon sensors for read-out in the China Jinping Underground Laboratory (CJPL), to search for neutrinoless double-beta decay of ^{82}Se , called the N ν DEx experiment. Besides located at CJPL with world's deepest rock shielding, N ν DEx combines the advantages of the high Q value (2.996 MeV) of ^{82}Se and TPC's ability to distinguish signal and background events using their different topological characteristics. These give N ν DEx unique and great potential for low background and high sensitivity.

N ν DEx-100, the N ν DEx experiment phase with 100 kg of SeF_6 gas, is being built and planned to complete with installation at CJPL around year 2025. This report will introduce the $0\nu\beta\beta$ physics, N ν DEx concept and its advantages, the schematic design of N ν DEx-100 and its sub-systems, as well as the background and sensitivity estimation for it.

KEYWORDS: neutrinoless double-beta decay, time projection chamber, $^{82}\text{SeF}_6$, China Jinping Underground Laboratory

¹Corresponding author.

Contents

1	The Physics	1
2	NνDEx Concept and its Advantages	2
3	NνDEx-100 Schematic Design	3
3.1	N ν DEx-100 Overall Design	3
3.2	Pressure Chamber and Inner Copper Shielding	4
3.3	Field Cage	7
3.4	Topmetal-S Sensor and Readout Plane	8
3.5	Data Acquisition	10
3.6	External Shielding	11
3.7	Gas System	12
3.8	Negative-pressure Clean Room	14
4	Background and Sensitivity Estimation	14
4.1	Natural Radioactive γ Background	14
4.2	Neutron Background	15
4.3	Cosmogenic Background	16
4.4	Other Backgrounds	19
4.5	Pile-up Event Background	21
4.6	Sensitivity Estimation	22
5	Summary	23

1 The Physics

The Standard Model (SM) of particle physics is an important cornerstone of physics and even the entire natural sciences, and has been successfully tested by experiments for more than half a century. The discovery of its last component, the Higgs particle, marked the perfect end of an era. In the SM, neutrinos have no mass. However their oscillations, which have been observed nowadays by many independent experiments and are supported by irrefutable evidence, require the presence of a mass term, non-diagonal in the flavor basis. This is the first experimental proof of physics beyond the SM that has been found in particle physics. To this day, some properties of neutrinos are still not known, such as whether they are Dirac or Majorana fermions, their absolute masses and mass hierarchy.

The charged fermions in the SM are all Dirac particles, which gain mass through Yukawa coupling with Higgs boson. Since neutrinos are electrically neutral, they are the only candidates in the SM to be Majorana fermions, *i.e.* they could be their own antiparticle. If this is the case, we can

also explain why their masses are so much lower than the ones of the other charged leptons in the SM by introducing a seesaw mechanism [1]. Neutrinoless double beta decay experiments are the ideal way to find out if this the the case: If such a process is observed, it would be an irrefutable proof that neutrinos are Majorana particles, which would open the door to new physics. The measured decay rate can quantitatively constrain the absolute mass and mass ordering of neutrinos. In addition, neutrinoless double beta decay violates lepton number and CP parity conservations, which can lead to the generation of net lepton number in the early universe evolution, and thereby may explain the matter-antimatter asymmetry in the universe.

2 NvDEx Concept and its Advantages

The rate at which neutrinoless double beta ($0\nu\beta\beta$) decay occurs (if it occurs) is extremely low, making experimental observations difficult. This kind of experiments has been developed for decades, and there is intense competition among various experimental approaches. Existing large-scale experiments include GERDA [2], MAJORANA [3], CUORE [4], CUPID [5], KamLAND-Zen [6], EXO [7], etc. In China, experiments including CDEX [8], PandaX [9], CUPID-China [10], and JUNO [11] have searched for or are being developed to search for $0\nu\beta\beta$ decay. Currently, the highest experimental half-life sensitivity reaches $10^{25} - 10^{26}$ years, yet the existence of such decay has not been observed. Next-generation $0\nu\beta\beta$ decay experiments are approaching the sensitivity needed for the case of inverted hierarchy of neutrino masses, on the order of 10^{27} years for most $0\nu\beta\beta$ decay isotopes. For the case of normal hierarchy of neutrino masses, which is slightly favored by oscillation experiment results so far, the required experimental half-life sensitivity is 2 orders of magnitude higher, on the order of about 10^{29} years.

The key to improving the sensitivity of neutrinoless double beta decay experiments is to reduce the experimental background. With zero background, the sensitivity of the experiment is proportional to the exposure (mass of decay isotope \times experiment time). However, in the presence of high background, experimental sensitivity increases only like the square root of exposure [12]. Thus to increase experimental sensitivity by another 1-3 orders of magnitude, innovative techniques must be applied to significantly reduce the experimental background.

The concept of “No neutrino Double-beta-decay Experiment (NvDEx)” experiment, searching for the neutrinoless double-beta decay of ^{82}Se using a high-pressure gas time projection chamber (TPC) with $^{82}\text{SeF}_6$ as the working medium and read out by Topmetal sensor chips, was proposed by D.R. Nygren, B.J.P. Jones, N. López-March, Y. Mei, F. Psihas and J. Renner in 2018 [13]. This scheme combines the high Q value of ^{82}Se with the ability of TPC to distinguish signal and background using event topology, which can greatly reduce the experimental background. The Q value of ^{82}Se decay is as high as 2.996 MeV, which is higher than most of the natural radioactive backgrounds, and also higher than that of the decay isotopes currently used in many mainstream experiments. For example, the natural radioactive γ background near the Q value of ^{82}Se is more than 2 orders of magnitude lower than that around the Q value of ^{136}Xe (2.458MeV). Meanwhile, in gaseous TPC, the double beta decay can be reconstructed as two electron tracks, each with a distinct Bragg peak at the end. This feature can be used to distinguish signal from background.

However, this experimental concept faces a major technical challenge: SeF_6 is an electronegative gas, in which the electrons generated by ionization will quickly be combined with gas molecules

to form negative ions, and electron avalanche amplification cannot happen. Thus with traditional technologies, the weak signals cannot be read out. To solve this problem, we designed the Topmetal-S sensor [14, 15], a kind of silicon sensor chip with a layer of metal on top, which is dedicated to $0\nu\beta\beta$ decay experiments, making TPC without physical amplification possible. It adopts industrial semiconductor CMOS process, and the top layer has a metal sheet for charge collection. In principle, its noise level can be as low as about 30 e-, thus the primary ionized charge can be directly read out without physical amplification. This gives us a unique opportunity to search for $0\nu\beta\beta$ decay using $^{82}\text{SeF}_6$ gas TPC.

The construction of China Jinping Underground Laboratory (CJPL) provides a unique opportunity for the development of $0\nu\beta\beta$ decay experiments. CJPL has the deepest natural rock shield in the world, and the second phase of CJPL is being constructed with world-class experimental space and low background environment. NvDEx will be developed at CJPL, taking full advantage of its low background level and large space.

3 NvDEx-100 Schematic Design

3.1 NvDEx-100 Overall Design

Currently, we are developing a NvDEx-100 experiment with 100kg of natural SeF_6 gas, the preliminary design of which is shown in Fig. 1. The main body of the experiment is in a pressure chamber, with feed-through flanges for gas, low-voltage, optical fibers and high-voltage. Inside the pressure chamber is an inner copper shielding to shield most of the external radiation. The core detector of the experiment - TPC - is installed in the barrel part of the chamber. It is composed of an insulating layer, a high-voltage plane, a field cage, and a readout plane. The readout plane consists of the focusing layer and the readout electronics layer on which the Topmetal-S sensor chips are mounted. In addition to the main body of the experiment, there are lead and high-density polyethylene (HDPE) external shieldings surrounding the pressure chamber, as well as auxiliary facilities such as the gas system, which are not shown in Fig. 1.

When the experiment runs, ^{82}Se (with a natural abundance of 8.7%) in SeF_6 gas undergoes a double beta decay, releasing two electrons. In the case of a neutrinoless double beta decay, the total energy of the two electrons is 2.996 MeV. These two electrons lose energy in the gas, ionize the gas, and form curved tracks due to scattering. At the ends of the two tracks, two Bragg peaks with the largest energy loss are formed. Due to the electronegativity of SeF_6 , the electrons generated by ionization quickly form negative ions with surrounding SeF_6 molecules. Finally a variety of SeF_N^\pm ions will be formed with certain fractions, including SeF_{0-5}^+ and $\text{SeF}_{5,6}^-$, which will drift to the two ends of the TPC in the electric field. After the $\text{SeF}_{5,6}^-$ ions reach the readout plane, their signal is read out. The drift velocities of SeF_5^- and SeF_6^- ions are different, hence the arrival times will be different as well. The time difference can be used to obtain the drift distance. The readout plane consists of the focusing layer and the readout electronics layer. The focusing layer is used to generate certain electric field structure that allows the drift charges to pass through small holes in it, and be collected with 100% efficiency at the $\sim 1\text{mm}^2$ -sized readout electrodes on the surface of the Topmetal-S chips. The Topmetal-S chips are located on the surface of the readout electronics layer. They will measure the charge and time of the signal and generate digital data, which are

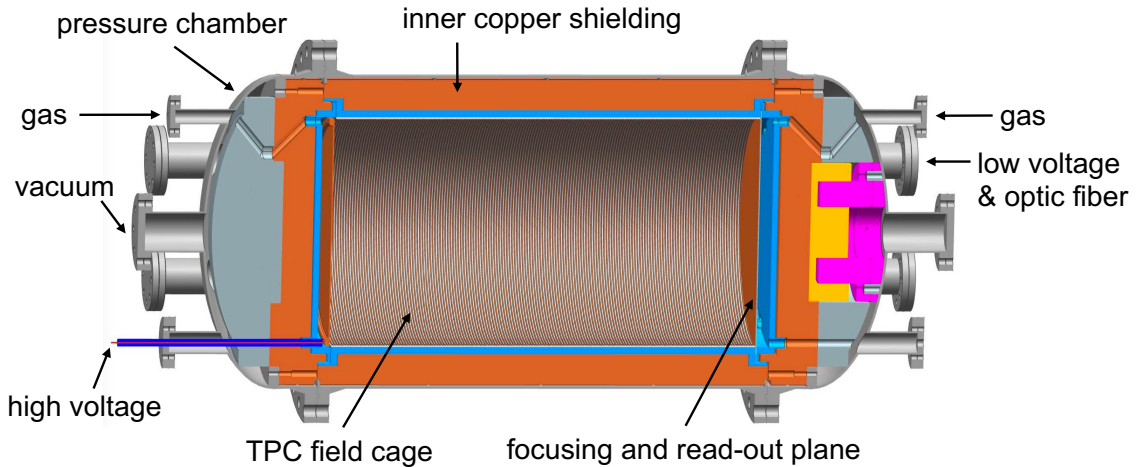


Figure 1. Schematic design of the main part of the NvDEx-100 experiment.

collected by the electronic readout boards, and transmitted to the data acquisition computer through the optical fibers.

3.2 Pressure Chamber and Inner Copper Shielding

NvDEx-100 will use SeF_6 gas at a pressure of 1.0 MPa. The design of the pressure chamber is shown in Fig. 2. The chamber consists of a barrel and two end caps, connected with two DN1200 Tongue-Grove (T-G) flanges. There are six smaller T-G flanges on each end cap: one DN50 flange for gas, one DN80 flange for high voltage, four DN125 flanges for low voltage and optic fibers, and one DN150 flange for vacuum. The inner diameter and length of the barrel are 1200 mm and 1760 mm, respectively. The chamber is made of 10mm-thick low background stainless steel. Figure 3 shows the cross-sectional view of the chamber. The weight of the chamber is around 2211 kg without taking the bolts into account. The barrel part of the pressure chamber sits on two saddles, while the two end caps are supported with carts, which can move away along the rails when opening the chamber.

In order to suppress the background radiation from outside the pressure chamber, a 12-cm thick oxygen free copper shielding with low radioactive isotope contamination will be placed inside the pressure chamber as shown in Fig. 1. Figure 4 is the cross-sectional view of the design of the inner copper shielding. It consists of a barrel part and two disks which will be mounted in the end cups of the pressure chamber. The outer and inner diameters of the barrel part are 1190 mm and 950 mm, respectively. The barrel part and the disks each weigh about 6108 kg and 1476 kg, respectively. There are some holes in the disks so that gas, optic fibers, low voltage cables and the high voltage feedthrough can go through. The holes, except the ones for high voltage, are tilted in order to avoid outside radiation reaching the sensitive volume of the TPC by a straight path.

The Topmetal sensors and electronics on the read-out plane will generate heat when taking data, which will induce convection in the SeF_6 gas in the sensitive volume, with maximum velocity larger than 10 cm/s assuming heat power of 700 W on the readout plane. This could be a problem

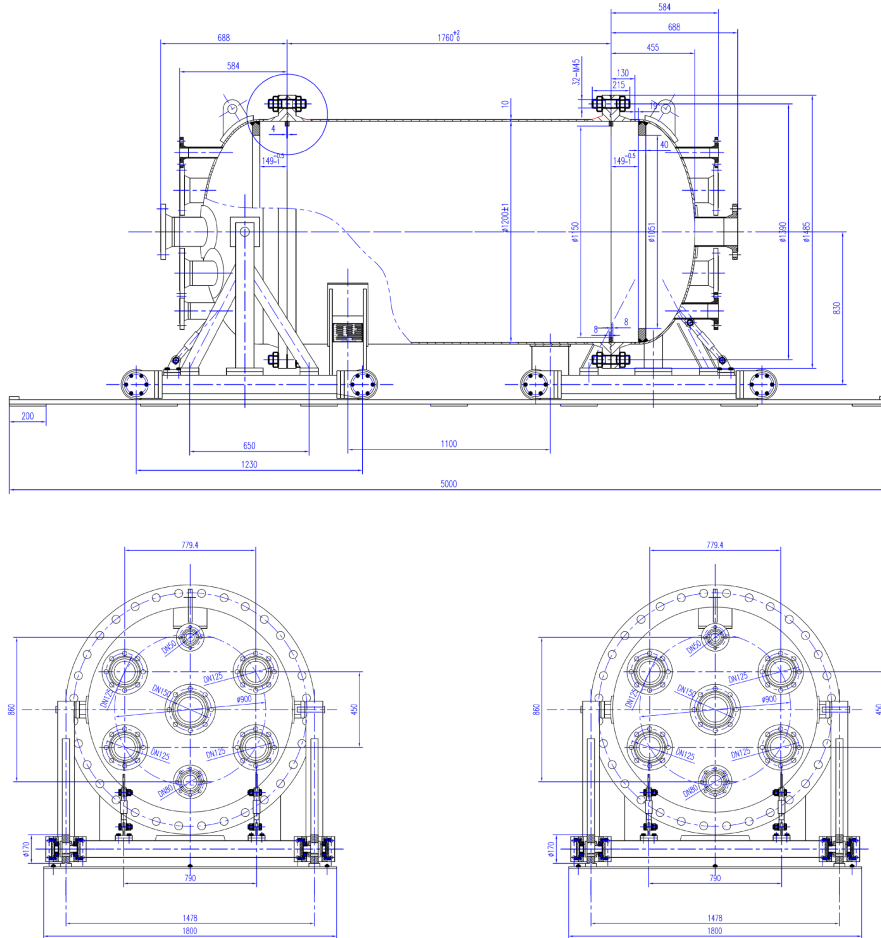


Figure 2. Design of the pressure chamber.

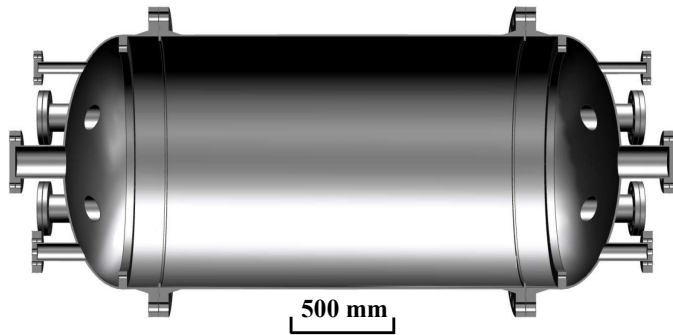


Figure 3. Cross-sectional view of the pressure chamber.

for NvDEx TPC, because the ions drift very slowly, with a velocity above 20 cm/s, which is much lower than the drift velocity of electrons (on the order of several cm/ μ s in most other TPC's), and the convection could cause serious distortion of the reconstructed event topology. It is thus necessary to cool the read-out plane and minimize the temperature difference inside the TPC. For

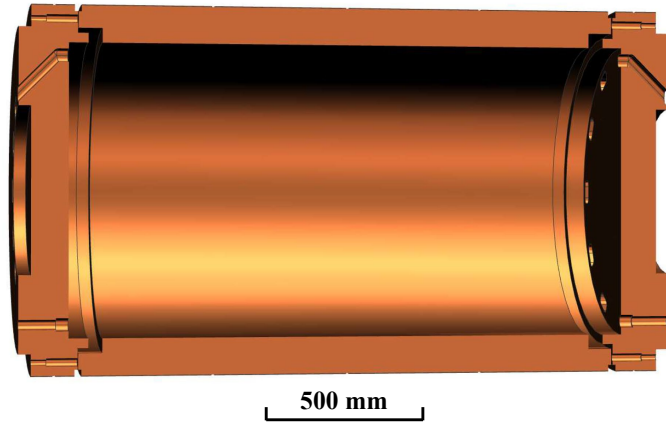


Figure 4. Cross-sectional view of the designed inner copper shielding.

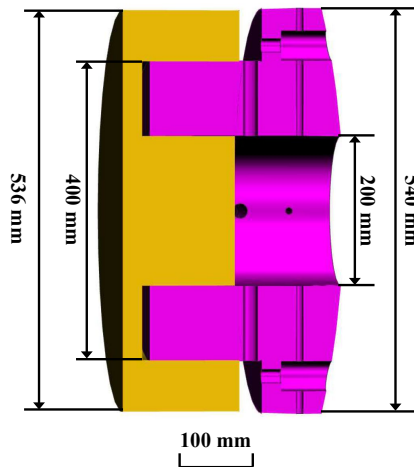


Figure 5. Cross-sectional view of the cooling base and tube.

for this purpose, a copper heat conductor will be placed between the inner copper shielding disk and the end cap of pressure vessel. As shown in Fig. 1, the heat conductor is composed of a base (in yellow) and a tube (in purple) fixed to the inner copper shielding disk and to the pressure chamber end cap, respectively. Figure 5 shows the cross-sectional view of the copper heat conductor with dimensions. The base and the tube can slide horizontally relative to each other. This design makes sure that there is good contact between all neighboring parts along the heat conduction path, even when the pressure chamber expands due to the gas pressure, so that the total heat resistance is at an acceptable level. The weight of the copper heat conductor is around 489 kg. A liquid cooling plate will be mounted on the outer surface of the end cup of the pressure chamber. The temperature difference in the TPC and convection in the gas will be minimized by adjusting the temperature of the cooling plate.

The SeF_6 and $^{82}\text{SeF}_6$ gases are very expensive. In order to reduce the amount of the gas to be used and the cost, two plastic fillers will be placed in the end caps of the the pressure chamber,

occupying the gap outside the inner copper shielding disks, as shown in Fig. 1. Since SeF_6 is toxic, any material that absorbs the gas and gradually releases it when the pressure chamber is open during the maintenance of the experiment could be a danger to people and the environment. Considering this, the fillers as well as the insulator layer and the TPC field cage supporting cylinder (to be described in the next subsection) will be made of polyoxymethylene (POM), which absorbs minimum amount of gas among plastic materials with acceptable mechanical strength. The design of the fillers is shown in Fig. 6. There are also some holes in the fillers for gas, optic fibers, low voltage cables and the high voltage feedthrough to go through.

Up to now, the pressure chamber and the inner copper shielding have been manufactured for an on-ground prototype experiment. The copper heat conductor as well as the fillers are being manufactured. The on-ground prototype will be assembled in the near future. Then tests will be carried out on gas tightness of the pressure chamber, heat conduction and temperature control of the read-out plane, etc.

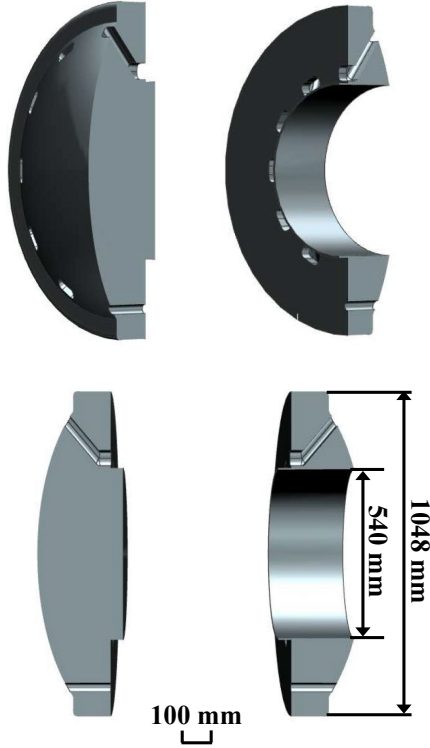


Figure 6. Cross-sectional view of the POM fillers.

3.3 Field Cage

The electronegativity of the SeF_6 gas used in NvDEx-100 is very high. This means the negatively charged particles drifting towards the readout plane will not be electrons, since they will be quickly captured, but negative ions instead. The readout plane will employ innovative Topmetal-S sensors to read out the drifted charge without physical amplification like electron avalanche. Details about Topmetal-S sensors and the readout plane will be introduced in Sub-section 3.4.

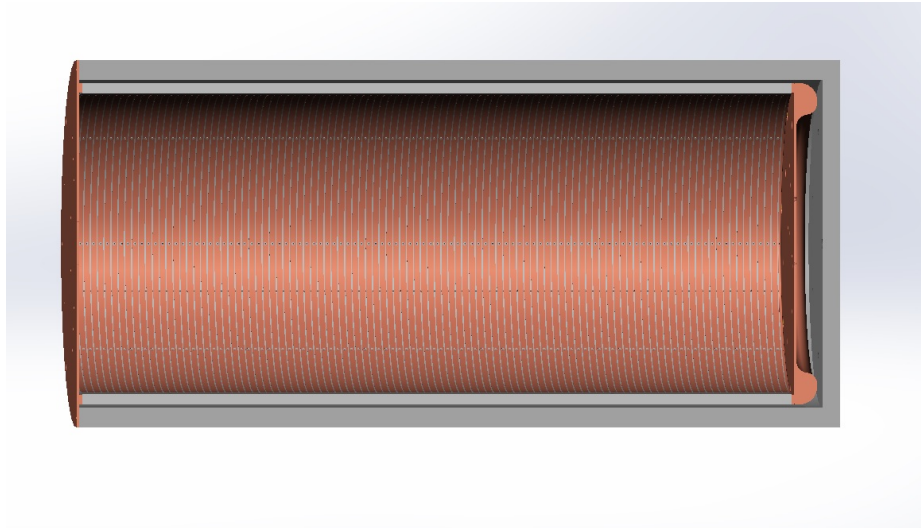


Figure 7. Cross-sectional view of the design of a prototype field cage.

Most of the drift negative ions will be SeF_6^- and SeF_5^- , however a number of more complex molecules may be formed. The drifting negative ions may form clusters like $\text{SeF}_6^-(\text{SeF}_6)_n$ and $\text{SeF}_5^-(\text{SeF}_6)_n$ ($n=1,2,3,\dots$) with low drift field. These clusters will smear the drift velocity of negative ions resulting in an increase of the noise. Similar to SF_6 , the cluster formation in SeF_6 can be suppressed with high drift fields. For this reason, the drift field of NvDEx-100 will be as high as 400V/cm, corresponding to a drift velocity of negative ions above 20cm/s.

A cross-sectional view of the design of a prototype field cage (FC) is shown in Fig. 7. The FC is isolated from the inner copper shielding by a 20mm-thick POM cylinder. The FC will be made of flexible printed circuit (FPC) sheets in the size of 315mm×423mm, each FPC has 5mm-wide copper strips with a pitch of 6mm on both sides. Three snap off holes at both ends and the center of each copper strip will be used to align and fix the FPC sheets onto a 10mm-thick POM supporting cylinder with screws. Two copper rings will be mounted at the two ends of the POM supporting cylinder. The copper strips and copper rings will be connected with low radioactive background resistors. The cathode of the TPC will be a low radioactive background copper plane mounted on the inner copper shielding disk, isolated with a POM layer of thickness 25mm. 8 pogopins will be used to ensure good connection between the cathode plane and the copper ring on the end of the cylinder part of the FC once the pressure chamber is closed.

A high voltage feedthrough will be connected to the cathode by spring pins. It is constructed using a compression seal approach, as shown in Fig. 8. A metal rod is pressed into a Polytetrafluoroethylene (PTFE) seal ring by clamping nuts on a DN80 flange. The feedthrough has been tested with high voltage of 100 kV and for leak-tightness in nitrogen at 1.0 MPa.

3.4 Topmetal-S Sensor and Readout Plane

Around 10k CMOS sensors, named Topmetal-S, arranged in an hexagonal pattern as shown in Fig. 9, will be directly placed at the site of charge measurement to collect ionization charges without avalanche multiplication. A perforated focusing electrode is placed above the readout plane with

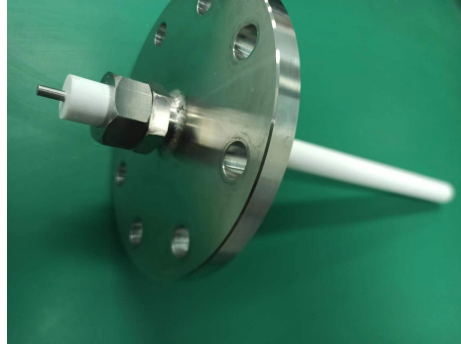


Figure 8. Image of the high voltage feedthrough.

round holes aligned with the charge collection electrodes on the Topmetal-S sensors concentrically. The focusing structure ensures all charges eventually land on the charge collection electrode for maximum charge collection efficiency.

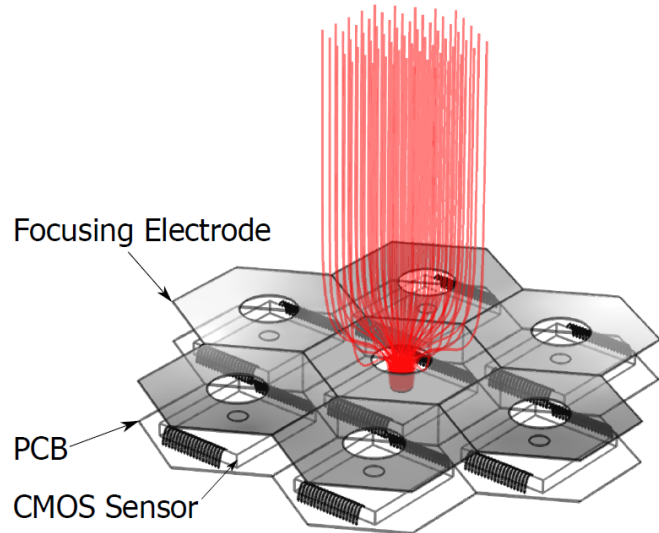


Figure 9. Topmetal-S sensors tiled in a hexagonal pattern to form a charge readout plane without gas gain.

Each Topmetal-S sensor is integrated with a charge collection electrode, a front-end amplifier and data processing circuits. The charge collection electrode is an exposed hexagonal top-most metal with a diameter of about 1 mm. The charge signal collected on the Topmetal electrode is directly DC coupled to the Charge Sensitive pre-Amplifier (CSA). The structure of the CSA in the prototype Topmetal-S sensor is a folded cascade amplifier with a feedback capacitor and a feedback transistor. The decay time of the CSA can be adjusted by changing the gate voltage of the feedback transistor.

Due to the stringent noise requirement, the analog signal of the CSA output must be digitized immediately. Thus an in-chip Analog-to-Digital Converter (ADC) is designed to minimize the transfer of the analog signal. The ADC should have a noise floor well below the noise of the CSA of about 1 mV and a large enough dynamic range to cover the possible range of input charge up

to about 40 ke^- . A sigma-delta (SD) ADC is used in the Topmetal-S sensor. It is composed of a SD modulator (analogue part) with coarse quantizers and decimation filter (digital part) together to produce a data-stream output. By sampling the input signal at a frequency that is much higher than the signal bandwidth (oversampling) the majority of the noise is shifted beyond the band of interest. The out-of-band noise is further attenuated by a decimation filter to achieve an improved signal-to-noise ratio. A photo of the Topmetal-S sensor chip is shown in Fig. 10.

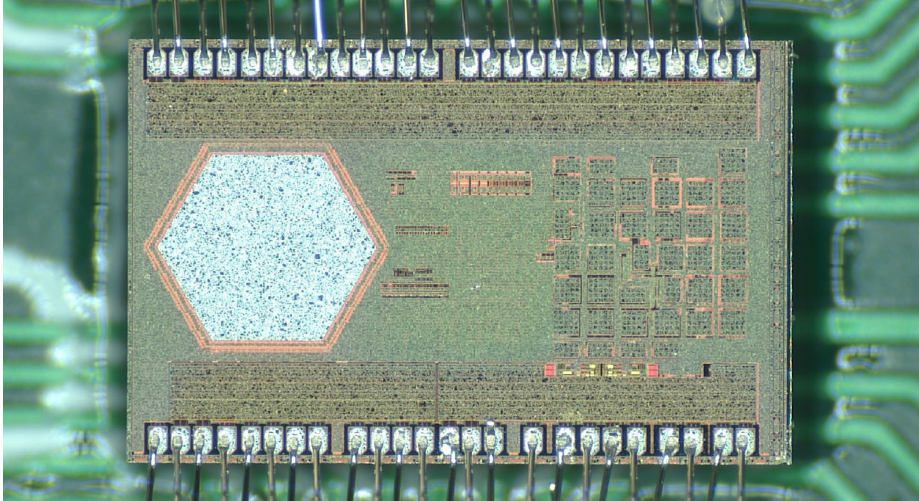


Figure 10. Photo of the Topmetal-S sensor chip.

Since the sensors are densely packed on the plane, the number of available paths for routing signal out of the plane is limited. Beyond certain plane size or total number of sensors, routing every signal from all sensors out becomes impractical. Digitized data must be communicated through inter-sensor network. Therefore, circuitry that handles data processing and communication must be integrated in the sensor. A distributed, self-organizing and fault-tolerant readout network is proposed with the Topmetal-S sensor. The proposed scheme forms a sensor network by establishing a local connection between adjacent sensors. Each sensor integrates a router as a node of the network, and hence each sensor not only generates and transmits its data but also forwards the data from its adjacent nodes. Finally the data are received by a data acquisition system, which is directly connected with the edge of the network and used to transmit the data between the sensor network and the computer.

3.5 Data Acquisition

With the two-dimensional distributed network formed by the digital part of the Topmetal-S sensors, the digitized waveform of each CSA output will be transmitted to the edge of the plane, in the way of streaming readout. The speed of the data chain could go up to 45 Mbps. As shown in Figure 11, the full plane is split into modules with different sizes, to cover the end-cap as much as possible. All the streaming data chains end in the modules on the right side, where the data are further encoded and aggregated into high-speed links with a speed of a few gigabits per second, by the commercial transceiver chips. Depending on orientation of the sensors and how the sensors on the edge columns are connected to the transceiver, there will be 20~50 bidirectional high-speed

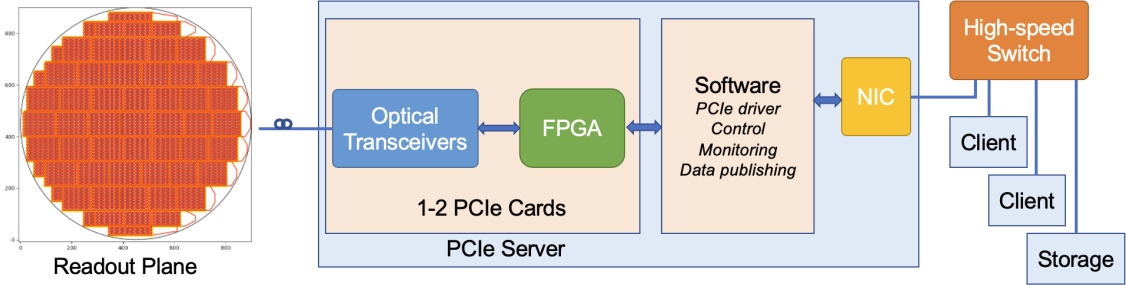


Figure 11. Architecture of the DAQ system.

links in total to connect the readout plan and the DAQ system in the back-end. In the other direction, the control data streams from the DAQ system are transmitted towards the left side of the readout plane.

The flexible Printed Circuit Board (PCB) modules will be fabricated with radiopure material. CMOS chips such as the Topmetal-S sensors are known to be low in radioactive contamination, while other components including the capacitors, resistors, transceivers and some power chips will be selected carefully. The radioactivity measurements will be done in the CJPL. Besides the material and components, any tools or materials used during the assembly procedures should also be clean enough.

In the back-end, a PCIe based DAQ system will be built to communicate with the front-end electronics on the readout plane via high-speed fiber optic links. Similar PCIe form factor has been adopted by dozens of large-scale experiments such as the ATLAS experiment at the LHC and the sPHENIX experiment at the RHIC [16, 17]. The streaming data from all sensors are received and decoded by FPGAs on the PCIe cards. The data processing, event building and filtering can be flexibly placed in the chain from the FPGA firmware to the software. The raw data and kinds of intermediate-stage data will be streamed from the DAQ server to a high-speed switch. Any client connected in the network can remotely subscribe the data and implement further data analysis.

3.6 External Shielding

In order to protect the NvDEEx detector from environmental radiations, an external lead shielding with a thickness of 20cm will be built outside the pressure chamber. The preliminary design of the external lead shielding is shown in Fig.12. It is composed of two mobile halves and a fixed base, on which the pressure chamber sits. The mobile halves, including the side walls and the top, are installed on a mobile base connected to a transmission system, so that they can move aside to enable opening and operations on the pressure chamber. The fixed base is installed on a vibration isolation system, in order to minimize influence on the experimental measurements from vibration. The vacuum and gas pipes, the high voltage cable, the low voltage cables and the optical fibers will pass the external lead shielding through several holes at the joints of the two mobile halves. Two shielding doors will be installed to prevent radiation from going through these holes directly. The lead bricks and the steel structure inside the lead layer will be tested and selected for radioactive contamination.

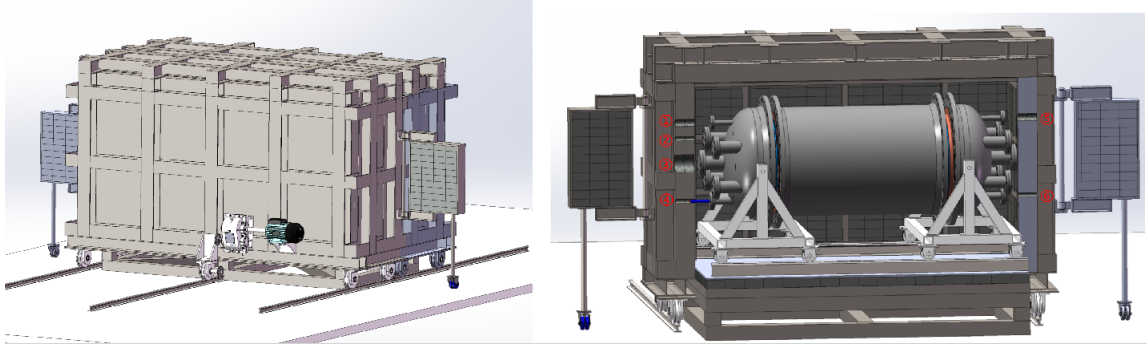


Figure 12. Design of the external shielding.

Lead is very effective at stopping external γ radiation, but it's not a good shielding material for neutrons. High-density polyethylene (HDPE) blocks will be placed in the gap between the pressure chamber and the external lead shielding, in order to slow down and absorb neutrons. The HDPE material will also be tested for radioactivity.

3.7 Gas System

The working medium of NvDEx is highly toxic SeF_6 gas. When there is moisture in it, SeF_6 can easily decompose and produce corrosive HF, which may damage detector components and / or cause leakage of the toxic gas. The gas system of NvDEx should be able to fill the pressure chamber with SeF_6 to the working pressure of 1 MPa, discharge the gas from the pressure chamber and safely store it during maintenance of the experiment. During the lifetime of the experiment, the pressure vessel will be pressurized, depressurized and vacuumized many times. And the pressure vessel and part of the gas system will be working at pressure of 1 MPa for years during data taking. Thus gas tightness and reliability is critical for NvDEx gas system.

With these considerations, the schematic of the NvDEx gas system is designed as shown in Fig. 13.

The pressure chamber is connected to a turbomolecular vacuum pump and a dry vacuum pump, which can vacuumize the chamber and the gas system before filling SeF_6 gas. This can minimize contamination of the SeF_6 gas by air, moisture, and Radon, in order to avoid corrosion and radiation background from the gas.

Every time before filling the toxic SeF_6 gas to the chamber, SF_6 , which has similar properties as SeF_6 but is non-toxic, is filled into the system with a pressure of 1 MPa to test the gas tightness of the pressure chamber and gas system. After the test, SF_6 will be compressed into a SF_6 storage tank to be used in the future.

In emergencies like gas leakage, fire, an earthquake, a power outage, etc., SeF_6 gas in the system will be released into an emergency pressure relief tank within 10 seconds, so that the pressure in the system is below atmospheric pressure, in order to ensure safety of personnel and environment.

Before maintenance of the experiment, SeF_6 gas will be discharged from the pressure chamber and condensed by the low temperature in a precooler and two condensers. After the SeF_6 saturated vapor pressure is reached in the system, a dry vacuum pump will further pump the gas from the pressure chamber to the condensers. Then the trace amount of SeF_6 left in the system will be

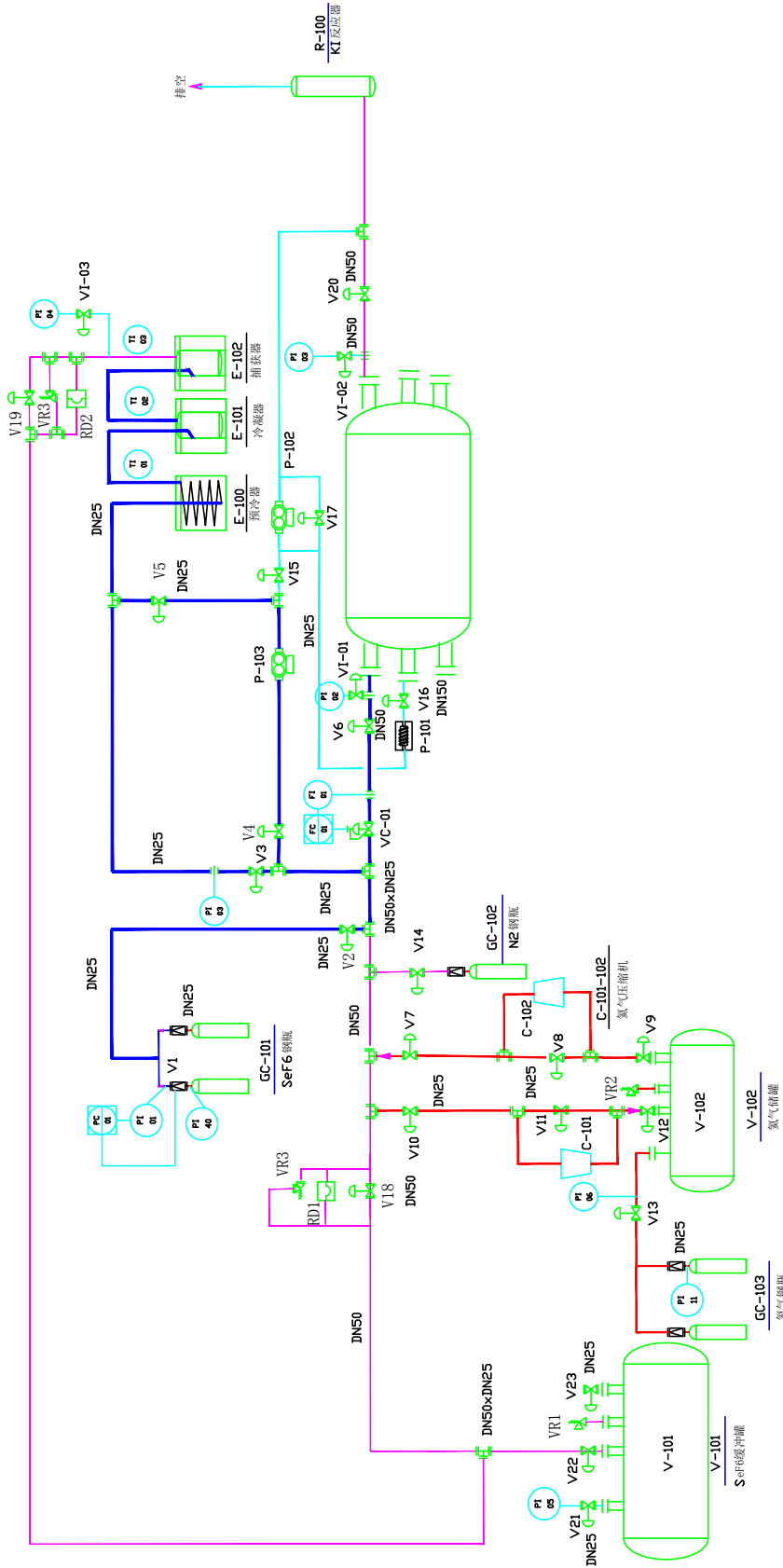


Figure 13. Schematic of the NvDEx gas system.

flushed by nitrogen gas into a KI reactor to be absorbed. And SeF_6 will be safely stored in the condensers at low temperature as solid and vapor at pressure below atmospheric pressure, which can be refilled to the pressure chamber in the future.

Up to now, all the components for the gas system have been purchased, waiting to be assembled once the experimental pressure chamber is finished with manufacture. Before moving to CJPL, the system will be commissioned and tested in the on-ground lab with SF_6 gas.

3.8 Negative-pressure Clean Room

A negative-pressure clean room will be built to install the whole experiment set-up inside. A clean class of 100,000 is required to avoid contamination of surfaces of the detector with dust, in order to control surface radioactive background. The negative pressure, together with a KI reactor at the exhaust vent of the clean room, serves as a second line of safety for the environment. In case any SeF_6 gas leakage happens, SeF_6 will flow with the air to the KI reactor and be absorbed. An environmental temperature of $22 \pm 2^\circ\text{C}$ is required to minimize gas convection in the TPC. And environmental humidity of $30 \pm 10\%$ is required to avoid condensation of moisture at cold spots, such as the cooling plate on the pressure chamber, on the experiment set-up.

4 Background and Sensitivity Estimation

4.1 Natural Radioactive γ Background

Radioactive isotopes are always present in the walls of the hall and in the rock surrounding them, as well as in the materials of the experimental set-up itself. The decays of these isotopes will produce a large amount of α , β and γ particles. The first two, however, will mostly be stopped without causing detectable background unless they are generated in or near the sensitive volume. So our main concern is the latter. γ that penetrate into the sensitive volume may interact with the gas and generate free electrons, which are visible to the detector. This is a major background source for NvDEx.

A 20cm-thick external lead shielding and a 12cm-thick inner copper shielding outside and in the pressure chamber are used to shield external γ 's. The thicknesses of the shielding layers are optimized using Geant4 simulations [18–20]. Due to the presence of radioactive contamination in the shielding materials themselves, the γ flux in the sensitive volume will not always decrease as the shielding thickness increases.

Most of the Region-Of-Interest (ROI) γ background comes from the decay of ^{214}Bi from ^{238}U decay chain. The probability of having a γ with energy larger than 2.9 MeV from a ^{214}Bi decay is 6.8×10^{-4} [21], which is quite rare. This is the advantage of ^{82}Se 's high Q value for NvDEx. The decay of ^{208}Tl from the ^{232}Th decay chain contributes about one order of magnitude less ROI background, with only around 8.5×10^{-5} [21] of the produced γ having energy around and above the ROI. Thus we will only focus on the ^{238}U decay chain in our γ background simulation and estimation.

The ^{238}U radiation activity of materials considered in our simulations are listed in table 1. The ^{238}U activity of the concrete in the experimental hall walls is from a measurement at CJPL [22]. The contribution of the rocks was negligible, since the contamination rate of the rocks is significantly

lower than the concrete. For other materials in the experiment set-up, we used the measurements from the NEXT experiment [23]. These numbers will be updated using measurements of materials for $\text{N}\nu\text{D}\text{Ex}$ in the future. The activity of the POM material used for TPC field cage is assumed to be the same as HDPE in NEXT. Many other parts or materials, e.g., the SeF_6 gas, the Topmetal-S sensors, the Flexible PCB used in the field cage and readout plane, the bolts on the pressure camber, and various steel supporting structures outside the pressure chamber, are not considered in the current simulation, because of their relative smaller sizes, lower background contributions, complication to built the geometry model, and / or lack of knowledge on their radioactive activities. Due to the above-mentioned reasons, the current background simulation only serves as a very rough estimation and gives some guidance to hardware developments.

Table 1. Activity assumed for each material

Material	Subsystem	^{238}U Activity (mBq/kg)
Concrete	Experimental hall	6.8×10^3 [22]
Lead	External shielding	0.37 [23]
HDPE	External shielding	0.23 [23]
Steel	Pressure vessel	1.9 [23]
Copper	Inner copper shielding	0.012 [23]
POM	Field cage	0.23 [23]

The results of the natural radioactive γ background simulation are reported in table 2. The largest contribution comes from the POM of the field cage because it is close to the sensitive gas volume. The total ROI γ background level is about 0.4 evts/yr. Note that like most other types of backgrounds to be described in the following sub-sections, this background can be further suppressed by one order of magnitude using a neural network considering event topology information [13], to the order of only 0.04 evts/yr in ROI.

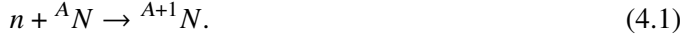
Table 2. γ background from different sources without suppression using event topology

Material	Subsystem	Background in ROI	
		evts/yr	10^{-5} evts/(keV kg yr)
Concrete	Experimental hall	0.004	0.12
Lead	External shielding	0.003	0.09
HDPE	External shielding	0.005	0.16
Steel	Pressure vessel	0.026	0.86
Copper	Inner copper shielding	0.050	1.67
POM	Field cage	0.330	10.99
Total		0.42	13.9

4.2 Neutron Background

Radioactive decays can emit neutrons as well. These events are quite rare, however, since it is significantly more difficult to stop neutrons than γ 's, the former can arrive more easily at the

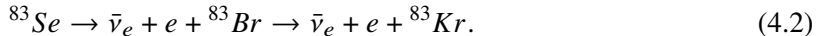
sensitive volume. Neutrons do not create ionization signals directly, but they can activate nuclei inside the detector, creating unstable isotopes via the reaction



Our main concern is if these isotopes will be created in the sensitive volume. The unstable isotopes we will consider are ${}^{83}\text{Se}$ and ${}^{20}\text{F}$, generated from ${}^{82}\text{Se}$ and ${}^{19}\text{F}$, respectively. In principle, other Se isotopes can also be created, but their Q-value is considerably lower than our ROI, so they will not provide additional background for the $0\nu\beta\beta$ decay search.

The main source of neutron induced background is ${}^{20}\text{F}$ with a β decay Q-value of 7.0 MeV. The fraction of the β spectrum that falls within the ROI is 9.4×10^{-3} , according to our Geant4 simulations.

${}^{83}\text{Se}$ decays via the chain reaction



The Q-value of ${}^{83}\text{Se}$ decay is 3.7 MeV. The fraction of β 's from ${}^{83}\text{Se}$ decay within our ROI is 2.7×10^{-5} , considerably less than the β 's from ${}^{20}\text{F}$ decay. This is because the ROI is in the tail of the β energy distribution. Our simulations show that the activation rate of ${}^{83}\text{Se}$ and ${}^{20}\text{F}$ are roughly the same, so we can safely ignore the former with subdominant ROI background contribution. The Q-value of ${}^{83}\text{Br}$ decay is 0.97 MeV, much lower than the ROI. Moreover, since its half-life is ~ 2.4 hours, it will not be a source of associated pile-up event background, either, so we can neglect it as well.

γ 's will be emitted from deexcitation of the products of the above β decays. However, the chance to have a high energy γ close to the ${}^{82}\text{Se}$ Q value is very low. Moreover, most of the emitted γ 's will pass through the gas volume without any ionization signals in the detector. If a γ interacts with the gas, in most cases, the TPC can separate its signal from the β decay signal in space, so that their energy will not be summed up to get a higher total energy.

Using Geant4 and FLUKA [24–27] packages, we simulated the neutron induced background rate. The fast neutron spectrum is assumed to be the one measured at CJPL and reported in [28]. Without the HDPE shielding, around 50 neutron activated background events / year is obtained within the ROI, which is even higher than the natural radioactive γ background.

The HDPE shielding is thus added to stop neutrons. Unlike high-Z materials like copper and lead, which can efficiently stop γ 's, HDPE contains a lot of hydrogen nuclei, which are able to slow down and absorb neutrons very effectively. HDPE blocks will be placed in the gap between the external lead shielding and the pressure vessel. The neutron induced background is then estimated as 0.1 events/year in ROI.

4.3 Cosmogenic Background

When materials used in the experiment are exposed to cosmic rays during production and transportation on the ground, they can be activated, creating relatively long-lived isotopes. The half-lives of these isotopes, although much shorter than those of ${}^{238}\text{U}$ and ${}^{232}\text{Th}$ described in Sub-section 4.1, can still be long enough, e.g. months to years, to make them an important background source even after the materials are placed underground.

The spallation process by high-energy cosmic nucleons is one of the dominant processes for the cosmogenic production of radionuclides. But other reactions like capture can also be important in some cases. Spallation reactions can produce a large number of radionuclides depending on the atomic number of the target material. On the Earth's surface, isotope production is dominated by neutrons because protons are absorbed by the atmosphere.

Cosmogenic activation can be minimized by reducing surface exposure, e.g. using shielding against the cosmic rays, avoiding flights and storing on the ground, or even producing materials underground. Purification techniques can also eliminate many of the induced isotopes. However, these preventive measures make the experiment preparation more complex. Consequently, it would be advisable to assess the relevance of the material exposure to cosmic rays for the experiments and its effect on the sensitivity. To quantify the induced activity, A , of an isotope with decay constant λ , both the production rate R of the isotope in the considered target, as well as the exposure history, must be well-known. In particular, A can be computed as:

$$A = R(1 - e^{-t_{exp}/\lambda})e^{-t_{cool}/\lambda} \quad (4.3)$$

considering t_{exp} the time of exposure to cosmic rays and t_{cool} the cooling time (time spent underground once shielded from cosmic rays).

Some direct measurements of production rates have been carried out for a few materials from the saturation activity, obtained by sensitive screening of materials exposed in well-controlled conditions. However, in many cases, production rates must be evaluated from the flux (per unit energy) of cosmic rays, ϕ , and the isotope production cross-section, σ , both depending on the particle energy E :

$$R = N_t \int \sigma(E)\phi(E)dE, \quad (4.4)$$

with N_t the number of target nuclei. We have used the ACTIVIA code [29] to calculate the cosmogenic activation for various materials used in $N\nu$ DEx. The cosmogenic activation rate of various radio-isotopes in SeF_6 gas, copper, lead and steel, as well as activities after exposure and cooling for certain time lengths, are shown in Tables 3, 4, 5, and 6. Only isotopes with relatively long half-lives and high Q-values are listed, since other isotopes will not create a background in $0\nu\beta\beta$ decay ROI after being placed underground for some cooling time.

As shown in Tab. 3, the most important cosmogenic background isotope from ^{82}Se is ^{56}Co , with Q-value of 4566 keV, which is above ^{82}Se Q-value, and a half-life of 77.3 days, which is long enough to remain a considerable activity of 0.02 $\mu\text{Bq}/\text{kg}$ after 2 years of exposure at sea level and 1 year of cooling time. Cobalt fluorides are solid rather than gas at room temperature, and so far we don't know whether or how much of the generated single-molecular ^{56}Co fluorides will remain in the gas after SeF_6 production, storage and transportation. Assuming conservatively that all the ^{56}Co stays in the gas and reaches the sensitive volume of the experiment, for 100kg of $^{82}\text{SeF}_6$ with ^{56}Co activity of 0.02 $\mu\text{Bq}/\text{kg}$, about 26 decays per year will happen. Thus energy deposition in ROI will be minimum.

Cosmogenic isotopes from ^{19}F , having mass numbers no larger than 19, do not have relatively large Q-value and long lifetime at the same time, thus will not constitute important cosmogenic background contributions.

Table 3. Cosmogenic activation rate of various radio-isotopes in enriched ^{82}Se , as well as activities after exposure at sea level and cooling for certain time lengths.

Isotope	Q-value (keV)	Half-life (d)	Production rate		Activity after 2yr exposure ($\mu\text{Bq}/\text{kg}$)	Activity after 1yr cooling ($\mu\text{Bq}/\text{kg}$)
			Calc.	Expt.		
^{54}Mn	1377	312	0.37	-	3.4	1.5
^{56}Co	4566	77.3	0.04	-	0.46	0.02
^{57}Co	836	272	0.14	-	1.4	0.54
^{58}Co	2307	70.9	0.83	-	9.6	0.27
^{60}Co	2824	1.92×10^3	0.11	-	0.29	0.26
^{75}Se	864	120	14.9	-	170	20.6

Table 4. Cosmogenic activation rate of various radio-isotopes in copper, as well as activities after exposure at sea level and cooling for certain time lengths.

Isotope	Q-value (keV)	Half-life (d)	Production rate		Activity after 2yr exposure ($\mu\text{Bq}/\text{kg}$)	Activity after 1yr cooling ($\mu\text{Bq}/\text{kg}$)
			Calc.	Expt.		
^{46}Sc	2367	83.8	3.1	2.18 ± 0.74	36	1.7
^{54}Mn	1377	312	14.3	8.85 ± 0.86	133	59
^{59}Fe	1565	44.5	4.2	18.7 ± 4.9	49	0.2
^{56}Co	4566	77.3	8.7	9.5 ± 1.2	101	3.8
^{57}Co	836	272	32.5	74 ± 17	318	125
^{58}Co	2307	70.9	56.6	67.9 ± 3.7	655	18
^{60}Co	2824	1.92×10^3	26.3	86.4 ± 7.8	71	62

The most important cosmogenic background isotope in copper is also ^{56}Co , as shown in Tab. 4. Considering that the inner copper shielding will be assembled and tested with the pressure chamber at the Institute of Modern Physics at Lanzhou, with an altitude of about 1500m, the exposed cosmic neutron flux is about 3.2 times higher than at sea level. The ^{56}Co activity will be about $323 \mu\text{Bq}/\text{kg}$ after 2 years of exposure. Using the simulation framework described in Sub-section 4.1, we find the ROI background in the sensitive volume from ^{56}Co emitted γ 's is as high as about 3700 evts / yr, which is much higher than the natural radiation γ background. After 3 years of cooling, the ROI background will drop to a subdominant level of 0.19 evts / yr. So it is important to place the inner copper shielding underground for cooling as early as possible.

Other isotopes in Table 4 have Q-value lower than ^{82}Se , so they will not contribute to the ROI background alone. However, since the drift velocity of ions in NvDEx TPC is slow, there is chance that ionization due to γ 's from these isotopes (or the ones coming from environmental radioactive decays) add up with other background sources, forming the so-called pile-up event backgrounds and reaching the ^{82}Se Q-value. This will be described in Subsection 4.5, taking ^{60}Co , which has a relatively long half-life and high Q-value, as an example of cosmogenic background isotopes.

As shown in Tables 5 and 6, the production rates of cosmogenic backgrounds in lead and steel

Table 5. Cosmogenic activation rate of various radio-isotopes in lead, as well as activities after exposure at sea level and cooling for certain time lengths. For short-lived isotopes with very long-lived parents (given in parentheses), we have considered the half-life of parent isotopes.

Isotope	Q-value (keV)	Half-life (d)	Production rate		Activity after 2yr exposure (μ Bq/kg)	Activity after 1yr cooling (μ Bq/kg)
			Calc.	Expt.		
^{56}Co	4566	77.3	0.026	–	0.30	0.01
^{57}Co	836	272	0.047	–	0.46	0.18
^{58}Co	2307	70.9	0.127	–	1.47	0.04
^{60}Co	2824	1.92×10^3	0.008	–	0.02	0.02
^{194}Au (^{194}Hg)	2501	1.90×10^5	5.52	–	0.17	0.17
^{202}Tl (^{202}Pb)	2398	1.93×10^7	120	–	0.04	0.04
^{207}Bi	1363	1.15×10^4	1.42	–	0.71	0.69

Table 6. Cosmogenic activation rate of various radio-isotopes in steel, as well as activities after exposure at sea level and cooling for certain time lengths.

Isotope	Q-value (keV)	Half-life (d)	Production rate		Activity after 2yr exposure (μ Bq/kg)	Activity after 1yr cooling (μ Bq/kg)
			Calc.	Expt.		
^{48}V	4012	16.0	21.6	–	250	3.4×10^{-5}
^{52}Mn	4712	5.59	40.0	–	463	1.0×10^{-17}
^{56}Co	4566	77.3	46.1	–	533	20
^{58}Co	2307	70.9	5.1	–	59	1.7
^{60}Co	2824	1.92×10^3	0.24	–	0.64	0.56
^{88}Y	3623	107	0.042	–	0.48	0.045

are either lower than or comparable to those in copper. Considering that they are shielded from the sensitive volume by the inner copper shielding, their background contribution should be less important than cosmogenic backgrounds in copper.

4.4 Other Backgrounds

We have also considered the following background categories for NvDEx, which are much lower than natural radioactive γ , neutron and cosmogenic backgrounds, and thus can be neglected:

- **Natural radioactive α and β background:** α and β from natural radioactive isotopes have much shorter path length than γ and neutrons. So they can influence the experiment measurement only if the radioactive isotopes are in the gas or on the surface to the sensitive volume. For the SeF_6 gas, since both the Se and F_2 gas materials are obtainable with high purity (99.999% for Se and 99.99% for F_2), the radioactive isotope contamination should be low. This needs to be further studied and confirmed by, e.g., ICP-MS measurements of the Se material, or future analysis of the data from NvDEx itself. Fluorides of U and Th are solids at room temperature. So far we don't know whether or how much of the U and

Th will stay in the gas and enter the sensitive volume after production, storage and filling of SeF_6 . Radioactive isotope contamination on the surface to the sensitive volume can be limited by careful cleaning of the components in the pressure chamber and gas system, especially directly on the surfaces to the sensitive volume, i.e., the inner surface of the field cage, the high voltage plate and the focusing plane. α and β from radioactive contamination on the surfaces to the sensitive volume can also be reduced by cutting the volume within a certain distance to the surface when analyzing the data, since the path length is within a few cm in the gas at 1 MPa.

- **Radon background:** Radon, as a radioactive gas which can be emitted from radioactive isotopes in the underground environment and in materials in the experiment set-up, may become a background source if it gets into the sensitive volume of the experiment. In order to limit the level of Radon contamination for the experiment, it is planned to have fresh air flushed through the clean room where the $\text{N}\nu\text{D}\text{Ex}$ experiment is located, during the assembling, running and maintaining of the experiment. Additionally, during the running of the experiment, the pressure chamber is air-tight with a gas pressure of 1 MPa inside, thus the amount of Radon penetrating into the chamber should be minimum. Radon can also be emitted from the materials inside the pressure chamber. Activated carbon can be placed in end caps of the pressure chamber outside the inner copper shielding, in order to absorb Radon. Both ^{222}Rn (half-life of 3.8 d) from the ^{238}U chain and ^{220}Rn (half-life of 55 s) from the ^{232}Th chain undergoes an alpha decay into polonium. A portion of the products in the following decay chain may be in the form of negative or positive ions, which will drift towards the anode or cathode in the electric field of the TPC. The α and β from the decay of Radon and its decay products (if they happen to not be ions and drift to the anode or cathode) will be further suppressed with event topology characteristics in TPC, since α forms thicker and straighter tracks than β and a single β event has 1 instead of 2 Bragg peaks. ^{214}Bi and ^{210}Tl in the ^{222}Rn decay chain have β decay endpoint energy above the ROI, thus could contribute to ROI background. Other α and β energies in the ^{222}Rn and ^{220}Rn decay chains are mostly away from the ^{82}Se Q value, further limiting the chance to create any background in the ROI. The γ from the decays of Radon and its decay products will have a small chance to interact with the gas, making a much smaller background contribution in ROI than the natural radioactive γ directly from the materials and environment mentioned in Sub-section 4.1.
- **Cosmic muon background:** As the deepest underground lab in the world, CJPL has a cosmic muon flux as low as $3.53 \pm 0.22 \text{ (stat.)} \pm 0.07 \text{ (sys.)} \times 10^{-10} \text{ cm}^{-2} \text{ s}^{-1}$ [30]. $\text{N}\nu\text{D}\text{Ex-100}$ as a meter-scale experiment at CJPL, will observe only the level of 0.3 cosmic muon per day. These muon background events will show straight tracks through the TPC and can be easily distinguished from $0\nu\beta\beta$ signal events, thus can be neglected. A very small fraction of muons will interact with the gas, creating some radioactive isotopes. The chance of this kind of background falling into the energy ROI is also neglectable considering the low muon flux at CJPL.
- **Neutrino scattering background:** Neutrinos from various sources can easily penetrate to the sensitive volume of the detector, but the chance a neutrino interacts with the gas is very

low. The most important contribution comes from solar neutrinos scattering with electrons, yielding backgrounds at a rate lower than the order of 0.1 evt/ROI/ton/yr [11]. These single electron background events will be further suppressed with event topology analysis as mentioned in Sub-section 4.1.

- **$2\nu\beta\beta$ decay background:** $2\nu\beta\beta$ decay events have exactly the same characteristics as $0\nu\beta\beta$ events except for lower energy. With the expected 1% FWHM energy resolution of NvDEx, $2\nu\beta\beta$ decay events will not be an important background source as shown in Fig. 14.

4.5 Pile-up Event Background

NvDEx-100 use a TPC as the main detector. The drift time for the about 160 cm maximum drift length is about 7s. If one event of the above-mentioned backgrounds happens, and while the ionization charges of this event drift, another background event also happens at the position near the cloud of the drifting charges from the first event, these two events could "pile-up" on each other, arriving at the read-out plane at the same location and the same time, looking like one event with energy equal to the total energy of these two events. Thus pile-up events tends to have higher energy than single background events. Since all kinds of background rate drop dramatically with increasing energy, pile-up events have a higher chance to fall into ROI than singal background events.

Here we do a very rough estimation of pile-up event background rate. We assume two events can be separated if they are 10cm×10cm×10cm away when the second event happens. 10cm is roughly the size of a $0\nu\beta\beta$ event in SeF_6 gas at the pressure of 1 MPa. Since events with lower energy, which dominates the background energy spectrum, are also smaller in size, this will be a conservative estimation. With this assumption, we take the single event energy spectra for various backgrounds, do a convolution and a proper normalization, and obtain the pile-up event background energy spectra in Fig. 14 and 15 for NvDEx-100 using natural SeF_6 gas and enriched $^{82}\text{SeF}_6$ gas, respectively.

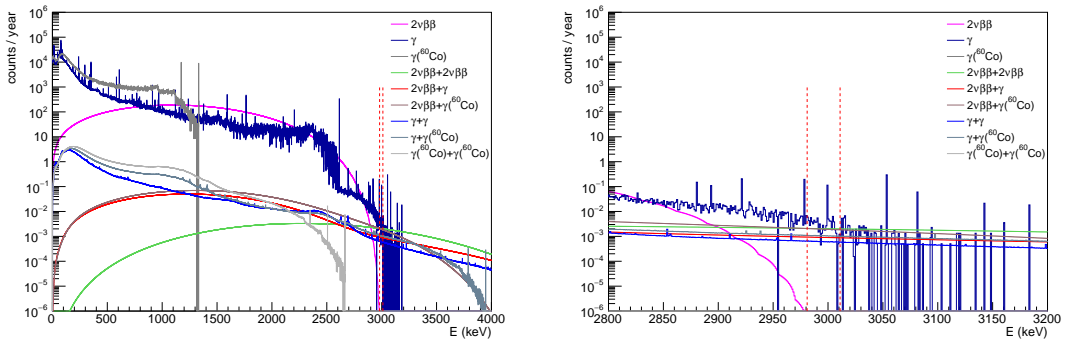


Figure 14. Energy spectra for various single-event and pile-up backgrounds of the NvDEx-100 experiment with natural SeF_6 gas without further suppression using event topology information.

As can be seen from the plots, for the NvDEx-100 experiment with natural SeF_6 gas, the highest pile-up background component is $2\nu\beta\beta + 2\nu\beta\beta$ background, which contributes to the level of 0.06 events per year in ROI. This is still lower than single-event natural radiation γ background.

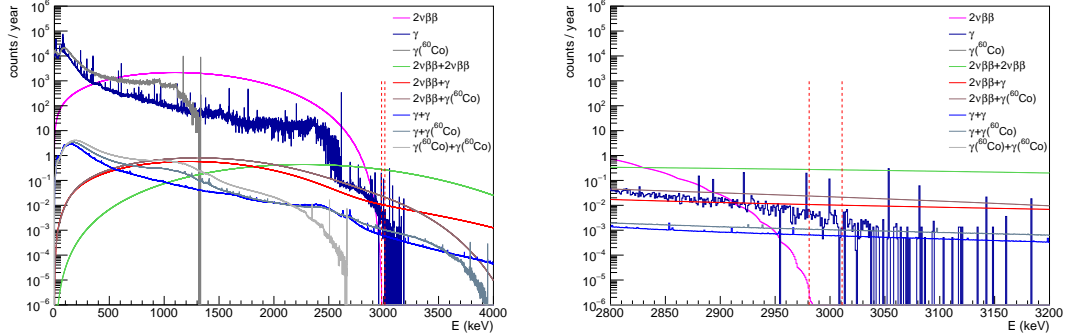


Figure 15. Energy spectra for various single-event and pile-up backgrounds of the NvDEx-100 experiment with enriched $^{82}\text{SeF}_6$ gas without further suppression using event topology information.

However, for the NvDEx-100 experiment with enriched $^{82}\text{SeF}_6$ gas, $2\nu\beta\beta + 2\nu\beta\beta$ pile-up background is at the level of 8 events per year in ROI, which is even higher single-event natural radiation γ background. Thus, suppression of pile-up backgrounds need to be considered in the future for the NvDEx-100 experiment with enriched $^{82}\text{SeF}_6$ gas. With full simulation of charge drift, diffusion and read-out responses, a more careful study of pile-up backgrounds can be conducted in the future, which will be more precise than the current conservative estimation. With neural network etc., event topology information can also be used to distinguish pile-up events from double-beta decay events, reducing pile-up events contribution. If the pile-up backgrounds can not be suppressed to be smaller than single-event γ background with only software, adding scintillation light detection at the HV plane side using silicon PM and light guides is also an option to explore in the future. To do this, the SeF_6 gas scintillation characteristics need to be studied. If needed, other scintillator gas may be mixed into the $^{82}\text{SeF}_6$ gas to increase the scintillation light yield. And the HV plane may also need to be changed to a mesh to allow scintillation light to go through. With scintillation light read-out, which can easily separate signals from 2 events happening several ns apart, pile-up background events can be almost completely rejected.

4.6 Sensitivity Estimation

If NvDEx-100 is successfully developed and reaches the background level listed above, the dominant background contribution are natural radiation γ background and neutron background, at the level of 0.4 and 0.1 cts / yr in ROI, respectively, before suppression using event topology information.

According to studies in [13], using event topology information the neural network can further suppress background by a factor of about 10 while keeping 90% signal efficiency. So the final background level is 0.05 cts / yr in ROI. In 5 years of running time, the background is about 0.25 counts in ROI. Thus NvDEx-100 is almost a zero-background experiment.

For simplicity, the NvDEx-100 experiment sensitivity is calculated assuming 0 background and shown in Fig.16. We can see that, using 100kg of natural SeF_6 gas, the $T_{1/2}$ sensitivity can reach 4×10^{25} yrs at 90% confidence level, after 5 years of running. If using enriched $^{82}\text{SeF}_6$ gas, the $T_{1/2}$ sensitivity can reach 4×10^{26} yrs at 90% confidence level after 5 years of running, which is better than the current best $T_{1/2}$ sensitivity of 2.3×10^{26} yrs from KamLAND-Zen experiment [6].

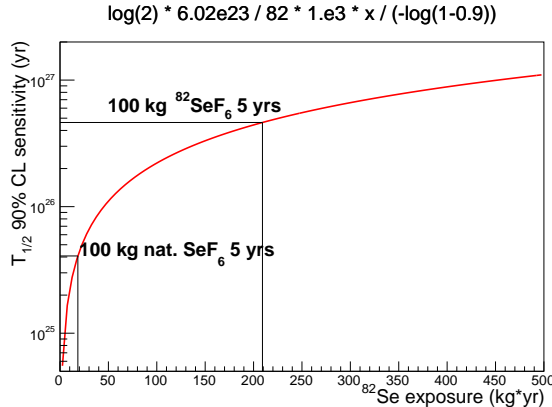


Figure 16. Estimated NvDEx-100 experiment sensitivity as a function of exposure.

5 Summary

In summary, NvDEx-100 is a 100-kg scale neutrinoless double-beta experiment using high-pressure SeF_6 gas TPC, which will be placed in the China Jinping Underground Laboratory. The topmetal-S sensors have been developed in order to read out drift ion signals in the NvDEx TPC with the electronegative SeF_6 gas. All sub-systems of NvDEx-100, including the pressure chamber and inner copper shielding, TPC field cage, readout plane and data acquisition system, external shielding, gas system, as well as the negative-pressure clean room, have been finished with conceptual design and are described in this report. NvDEx-100 is being built and planned to complete with installation at CJPL around year 2025. Combining the advantages of the high Q value (2.996 MeV) of ^{82}Se and TPC's ability to distinguish signal and background events using their different topological characteristics, NvDEx-100 can achieve very low background level of 0.05 cts / yr in ROI and high $T_{1/2}$ sensitivity of 4×10^{25} (4×10^{26}) yrs at 90% confidence level after 5 years of running, using 100 kg of natural SeF_6 (enriched $^{82}\text{SeF}_6$) gas.

Acknowledgments

This project is supported by the National Key Research and Development Program of China 2021YFA1601300 and 2022YFA1604703, From-0-to-1 Original Innovation Program of Chinese Academy of Sciences ZDBS-LY-SLH014, and International Partner Program of Chinese Academy of Sciences GJHZ2067.

References

- [1] Rabindra N. Mohapatra and Goran Senjanovic. Neutrino Mass and Spontaneous Parity Non-conservation. *Phys. Rev. Lett.*, 44:912, 1980.
- [2] M. Agostini et al. Final Results of GERDA on the Search for Neutrinoless Double- β Decay. *Phys. Rev. Lett.*, 125(25):252502, 2020.

- [3] C. E. Aalseth et al. Search for Neutrinoless Double- β Decay in ^{76}Ge with the Majorana Demonstrator. *Phys. Rev. Lett.*, 120(13):132502, 2018.
- [4] D. Q. Adams et al. Search for Majorana neutrinos exploiting millikelvin cryogenics with CUORE. *Nature*, 604(7904):53–58, 2022.
- [5] C. Augier et al. Final results on the $0\nu\beta\beta$ decay half-life limit of ^{100}Mo from the CUPID-Mo experiment. *Eur. Phys. J. C*, 82(11):1033, 2022.
- [6] S. Abe et al. Search for the Majorana Nature of Neutrinos in the Inverted Mass Ordering Region with KamLAND-Zen. *Phys. Rev. Lett.*, 130(5):051801, 2023.
- [7] G. Anton et al. Search for Neutrinoless Double- β Decay with the Complete EXO-200 Dataset. *Phys. Rev. Lett.*, 123(16):161802, 2019.
- [8] Li Wang et al. First results on ^{76}Ge neutrinoless double beta decay from CDEX-1 experiment. *Sci. China Phys. Mech. Astron.*, 60(7):071011, 2017.
- [9] Kaixiang Ni et al. Searching for neutrino-less double beta decay of ^{136}Xe with PandaX-II liquid xenon detector. *Chin. Phys. C*, 43(11):113001, 2019.
- [10] Ming-Xuan Xue, Yun-Long Zhang, Hai-Ping Peng, Zi-Zong Xu, and Xiao-Lian Wang. Study of CdMoO_4 crystal for a neutrinoless double beta decay experiment with ^{116}Cd and ^{100}Mo nuclides. *Chin. Phys. C*, 41(4):046002, 2017.
- [11] Jie Zhao, Liang-Jian Wen, Yi-Fang Wang, and Jun Cao. Physics potential of searching for $0\nu\beta\beta$ decays in JUNO. *Chin. Phys. C*, 41(5):053001, 2017.
- [12] J. J. Gomez-Cadenas, J. Martin-Albo, M. Sorel, P. Ferrario, F. Monrabal, J. Munoz-Vidal, P. Novella, and A. Poves. Sense and sensitivity of double beta decay experiments. *JCAP*, 06:007, 2011.
- [13] D. R. Nygren, B. J. P. Jones, N. López-March, Y. Mei, F. Psihas, and J. Renner. Neutrinoless Double Beta Decay with $^{82}\text{SeF}_6$ and Direct Ion Imaging. *JINST*, 13(03):P03015, 2018.
- [14] Chaosong Gao, Mangmang An, Guangming Huang, Xing Huang, Yuan Mei, Quan Sun, Xiangming Sun, Le Xiao, and Ping Yang. A Low-Noise Charge-Sensitive Amplifier for Gainless Charge Readout in High-Pressure Gas TPC. *PoS*, TWEPP2018:083, 2019.
- [15] Bihui You, Le Xiao, Xiangming Sun, Yuan Mei, and Guangming Huang. A distributed readout network ASIC for high-density electrode array targeting at neutrinoless double-beta decay search in a Time Projection Chamber. *Nucl. Instrum. Meth. A*, 988:164871, 2021.
- [16] J. Anderson, K. Bauer, A. Borga, H. Boterenbrood, H. Chen, K. Chen, G. Drake, M. Dönszelmann, D. Francis, D. Guest, B. Gorini, M. Joos, F. Lanni, G. Lehmann Miotto, L. Levinson, J. Narevicius, W. Panduro Vazquez, A. Roich, S. Ryu, F. Schreuder, J. Schumacher, W. Vandelli, J. Vermeulen, D. Whiteson, W. Wu, and J. Zhang. Felix: a pcie based high-throughput approach for interfacing front-end and trigger electronics in the atlas upgrade framework. *Journal of Instrumentation*, 11(12):C12023, dec 2016.

- [17] K. Chen, H. Chen, J. Huang, F. Lanni, S. Tang, and W. Wu. A generic high bandwidth data acquisition card for physics experiments. *IEEE Transactions on Instrumentation and Measurement*, 69(7):4569–4577, 2020.
- [18] John Allison et al. Geant4 developments and applications. *IEEE Trans. Nucl. Sci.*, 53:270, 2006.
- [19] S. Agostinelli et al. GEANT4—a simulation toolkit. *Nucl. Instrum. Meth. A*, 506:250–303, 2003.
- [20] J. Allison et al. Recent developments in Geant4. *Nucl. Instrum. Meth. A*, 835:186–225, 2016.
- [21] D.A. Brown, M.B. Chadwick, R. Capote, et al. ENDF/B-VIII.0: The 8th major release of the nuclear reaction data library with CIELO-project cross sections, new standards and thermal scattering data. *Nuclear Data Sheets*, 148:1 – 142, 2018. Special Issue on Nuclear Reaction Data.
- [22] H. Ma, Z. She, W. H. Zeng, Z. Zeng, M. K. Jing, Q. Yue, J. P. Cheng, J. L. Li, and H. Zhang. In-situ gamma-ray background measurements for next generation CDEX experiment in the China Jinping Underground Laboratory. *Astropart. Phys.*, 128:102560, 2021.
- [23] V. Alvarez et al. NEXT-100 Technical Design Report (TDR): Executive Summary. *JINST*, 7:T06001, 2012.
- [24] T. T. Böhlen, F. Cerutti, M. P. W. Chin, A. Fassò, A. Ferrari, P. G. Ortega, A. Mairani, P. R. Sala, G. Smirnov, and V. Vlachoudis. The FLUKA Code: Developments and Challenges for High Energy and Medical Applications. *Nucl. Data Sheets*, 120:211–214, 2014.
- [25] Alfredo Ferrari, Paola R. Sala, Alberto Fasso, and Johannes Ranft. FLUKA: A multi-particle transport code (Program version 2005). 10 2005.
- [26] Giuseppe Battistoni et al. Overview of the FLUKA code. *Annals Nucl. Energy*, 82:10–18, 2015.
- [27] C. Ahdida et al. New Capabilities of the FLUKA Multi-Purpose Code. *Front. in Phys.*, 9:788253, 2022.
- [28] Qingdong Hu et al. Neutron background measurements at China Jinping underground laboratory with a Bonner Multi-sphere Spectrometer. *Nucl. Instrum. Meth. A*, 859:37–40, 2017.
- [29] J.J. Back and Y.A. Ramachers. Activia: Calculation of isotope production cross-sections and yields. *Nuclear Instruments and Methods in Physics Research Section A: Accelerators, Spectrometers, Detectors and Associated Equipment*, 586(2):286–294, 2008.
- [30] Ziyi Guo et al. Muon flux measurement at China Jinping Underground Laboratory. *Chin. Phys. C*, 45(2):025001, 2021.